

If

$$C_w = -4 \left[ \frac{Z_3/k}{1 - \exp(-2\pi Z_3/k)} \right]^{1/2},$$

one gets

$$\frac{\partial W_1}{\partial Z_1} = W \left[ i \frac{Z_3}{k} \frac{\partial L(Z_1)}{\partial Z_1} + \left( i - \frac{Z_3}{k} \right) \frac{\partial E(Z_1)}{\partial Z_1} \right] + \frac{C_w \exp[-Z_3 E(Z_1)/k]}{S^3(Z_1) R^{3/2}(Z_1)} \\ \times \exp\{i[(Z_3/k)L(Z_1) + E(Z_1)]\} \{ S(Z_1) R(Z_1) [\partial f(Z_1)/\partial Z_1 + i\partial g(Z_1)/\partial Z_1] - G(Z_1) \},$$

with

$$G(Z_1) = [f(Z_1) + ig(Z_1)] \{ 4Z_1 R(Z_1) + \frac{1}{2} [S(Z_1)] \partial R(Z_1) / \partial Z_1 \}.$$

The noted derivatives are as follows:

$$\begin{aligned} \partial f(Z_1) / \partial Z_1 &= k^2 - A^2 - 3Z_1^2 + 2Z_1 Z_3, \\ \partial g(Z_1) / \partial Z_1 &= g(Z_1) / Z_1 + 2kZ_1, \\ \partial L(Z_1) / \partial Z_1 &= 2Z_1 / R(Z_1) S(Z_1) [R(Z_1) - (A^2 + Z_1^2 + k^2) S(Z_1)], \\ \partial S(Z_1) / \partial Z_1 &= 2Z_1, \\ \partial E(Z_1) / \partial Z_1 &= -2k(Z_1^2 - A^2 + k^2) / R(Z_1), \\ \partial R(Z_1) / \partial Z_1 &= 4Z_1(A^2 + Z_1^2 + k^2). \end{aligned}$$

## Lamb Shift in the $(\text{Li}^6)^{++}$ Ion\*

C. Y. FAN† AND M. GARCIA-MUNOZ

*The University of Chicago, Enrico Fermi Institute for Nuclear Studies, Chicago, Illinois*

AND

I. A. SELLIN

*New York University, Department of Physics, New York, New York*

(Received 13 March 1967)

The energy difference between the  $2S_{1/2}$  and  $2P_{1/2}$  levels of the hydrogen-like atom  $(\text{Li}^6)^{++}$  was determined by measuring the lifetime of the metastable  $2S_{1/2}$  state in an electrostatic field (Stark quenching). The metastable ions were produced by charge equilibrating a lithium beam of energy  $\sim 3$  MeV in nitrogen gas and were then directed through the electrostatic field (about 10 kV/cm) between a pair of parallel plates. The field mixed the  $2S_{1/2}$ ,  $2P_{1/2}$ , and  $2P_{3/2}$  states and the photons from the subsequent decay from  $2P$  to the ground state were detected with two thin-window GM counters, one of them fixed and the other movable along the quenching chamber in the beam direction. From the normalized counting rates of the movable counter and the separation between the two counters, the lifetime of the perturbed  $2S$  state could be determined. It was found to be  $(2.629 \pm 0.021) \times 10^{-9}$  sec and  $(1.764 \pm 0.035) \times 10^{-9}$  sec for the field strengths  $7425 \pm 2$  and  $9173 \pm 2$  V/cm, respectively. From these values, the Bethe-Lamb theory of Stark quenching yields an averaged Lamb shift in the  $(\text{Li}^6)^{++}$  ion of  $63\,031 \pm 327$  Mc/sec. This result agrees with the theoretical value  $62\,740 \pm 47$  Mc/sec recently calculated by Erickson.

### I. INTRODUCTION

**I**N a series of high-precision experiments using microwave techniques, the energy difference between the  $2S_{1/2}$  and  $2P_{1/2}$  level of a hydrogen atom was established by Lamb and his collaborators at  $1057.77 \pm 0.10$

Mc/sec.<sup>1-6</sup> The corresponding shift in a  $\text{He}^+$  ion was also measured precisely as  $14\,040.2 \pm 4.5$  Mc/sec.<sup>7,8</sup> These deviations from the prediction of the Dirac

\* This work was supported in part by the National Aeronautics and Space Administration under Contract No. NsG179-61 and in part by the U.S. Atomic Energy Commission under Contract No. AT(11-1)-238.

† Present address: Department of Physics, University of Arizona, Tucson, Arizona.

<sup>1</sup> W. Lamb, Jr., and R. Retherford, Phys. Rev. **79**, 549 (1950).

<sup>2</sup> W. Lamb, Jr., and R. Retherford, Phys. Rev. **81**, 222 (1951).

<sup>3</sup> W. Lamb, Jr., Phys. Rev. **85**, 259 (1952).

<sup>4</sup> W. Lamb, Jr., and R. Retherford, Phys. Rev. **86**, 1014 (1952).

<sup>5</sup> R. Triebwasser, E. Dayhoff, and W. Lamb, Jr., Phys. Rev. **89**, 98 (1953).

<sup>6</sup> E. Dayhoff, S. Triebwasser, and W. Lamb, Jr., Phys. Rev. **89**, 196 (1953).

<sup>7</sup> W. Lamb, Jr., and M. Skinner, Phys. Rev. **78**, 539 (1950).

<sup>8</sup> E. Lipworth and R. Novick, Phys. Rev. **108**, 1434 (1957).

theory were first explained by Bethe<sup>9</sup> as due to the interaction of the atomic electrons with radiation fields. While there is every reason to believe that quantum electrodynamics is adequate to predict the level shifts, there exist small but persistent discrepancies between the theoretical and experimental values.<sup>1-11</sup> It is, therefore, important to measure the level shift in new atomic species in order to uncover the source of the present discrepancies.<sup>12-14</sup> In particular, since the theoretical values were obtained from quantum electrodynamics as a series in the quantity  $\alpha Z$ , where  $\alpha$  is the fine-structure constant and  $Z$  is the nuclear charge, a precise measurement of the shift in hydrogenlike atoms of higher nuclear charge will be a sensitive test of the relative importance of higher-order terms in  $\alpha Z$ .

The experimental method used by Lamb *et al.* can be illustrated by the block diagram shown in Fig. 1. A beam of atomic hydrogen is produced in a  $\text{H}_2$  dissociator and collimated into a region where some of the atoms are excited by electronic bombardment to the  $2S_{1/2}$  level. These atoms then pass through a rf resonance cavity before they reach the detector system. When the radio frequency coincides with the level difference between  $2S_{1/2}$  and  $2P_{1/2}$ , the quenching rate of the  $2S_{1/2}$  atoms reaches a maximum, and thus the radio frequency gives the value of the level shift of the  $2S_{1/2}$  and  $2P_{1/2}$  states.

Although a similar method was successfully used for the measurement of the level shift in the  $\text{He}^+$  ion,<sup>7,8</sup> two practical difficulties prevent the extension of the use of the same principle for the measurement in higher  $Z$  atoms. The first is to obtain a beam of single-electron atoms of nuclear charge  $Z > 2$  with a workable intensity, and the second is to construct a stable rf supply which can give sufficient high power at frequency  $\gtrsim 63\,000$  Mc/sec (the theoretical value of the Lamb shift in  $\text{Li}^{++}$  is  $\sim 62\,740$  Mc/sec) to quench the metastable atom. As a result, one is forced to approach the problem from entirely different directions.

It is well known that in a dc electric field, the Stark effect will mix mainly the  $2S_{1/2}$ ,  $2P_{1/2}$ , and  $2P_{3/2}$  states, thereby causing the  $2S_{1/2}$  metastable atoms to decay to the  $1S$  state accompanied by the emission of Lyman  $\alpha$ -like photons. The lifetime of the  $2S_{1/2}$  atoms is a

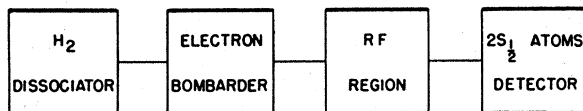


FIG. 1. Schematic block diagram of the apparatus used by Lamb and his collaborators for the level-shift measurement.

<sup>9</sup> H. Bethe, Phys. Rev. **72**, 339 (1947).

<sup>10</sup> R. T. Robiscoe, Phys. Rev. **138**, A22 (1965).

<sup>11</sup> A. Petermann, Fortsch. Physik **6**, 505 (1958).

<sup>12</sup> M. Leventhal, K. R. Lea, and W. E. Lamb, Jr., Phys. Rev. Letters **15**, 1013 (1965).

<sup>13</sup> K. R. Lea, M. Leventhal, and W. E. Lamb, Jr., Phys. Rev. Letters **16**, 163 (1966).

<sup>14</sup> C. Y. Fan, M. Garcia-Munoz, and I. A. Sellin, Phys. Rev. Letters **15**, 15 (1965).

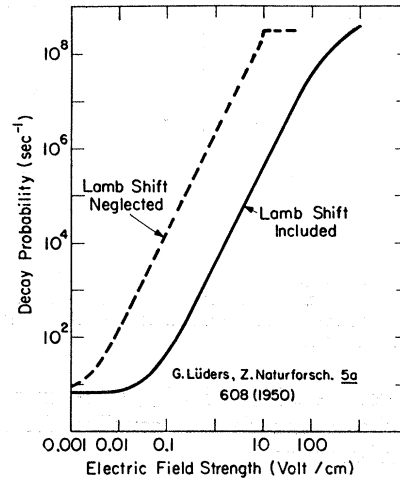


FIG. 2. Decay probability of  $2S_{1/2}$ -state hydrogen atoms in an electrostatic field (Stark quenching).

sensitive function of the level difference between  $2P_{1/2}$  and  $2S_{1/2}$ , the Lamb shift. Figure 2 shows the decay probability for a hydrogen  $2S_{1/2}$  atom as a function of the strength of the electrostatic field calculated by Lüders,<sup>15</sup> indicating the effect of the Lamb shift. It is clear that this property can then be turned into a new method of measuring the Lamb shift by measuring the lifetime of the  $2S_{1/2}$  atoms in a known electrostatic field. This is the principle which we used for the measurement of the Lamb shift in  $(\text{Li}^6)^{++}$  ions.<sup>14</sup>

In 1965 a brief article on the result of the preliminary experiments was published.<sup>14</sup> In this paper, which is an amplified version of Ref. 14, we shall (1) set forth the theoretical account for the experimental method, (2) describe the apparatus in detail, with estimates of uncertainties in the experimental results introduced from various factors, (3) list the best experimental results thus far obtained, and (4) give a short account on the comparison of the results with the theory. Although the accuracy of the results is not as high as one wishes, the experimental method nevertheless points to the possibility of determining Lamb shift in atoms of nuclear charge higher than that of Li. Work along this direction is under way.

## II. CONNECTION BETWEEN THE LIFETIME AND THE LAMB-SHIFT. PRINCIPLE OF THE EXPERIMENTAL METHOD

In the first approximation, the decay probability  $\gamma_s$  of a  $2S_{1/2}$ -state hydrogenlike atom in an electrostatic field  $E$  due to Stark mixing of  $2S_{1/2}$  and  $2P_{1/2}$  states is given by<sup>16</sup>

$$\gamma_s = \gamma |V|^2 / \hbar^2 (\omega_{bc}^2 + \frac{1}{4}\gamma^2), \quad (1)$$

where  $\hbar$  is the Planck constant divided by  $2\pi$ ,  $\gamma$  is the decay probability of the  $2P_{1/2}$  state,  $\omega_{bc}$  is the level

<sup>15</sup> G. Lüders, Z. Naturforsch. **5a**, 608 (1950).

<sup>16</sup> See Eq. (7) of Ref. 1, p. 561.

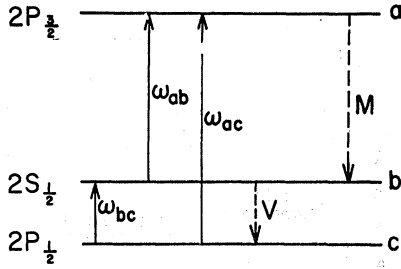


FIG. 3. Level diagram of a hydrogenlike atom, where  $\omega_{ab}$ ,  $\omega_{bc}$ , and  $\omega_{ac}$  are the energy differences of the levels in frequencies and  $V$  and  $M$  are the matrix elements of the Stark-effect coupling the corresponding states.

shift between the  $2S_{1/2}$  and  $2P_{1/2}$  states in frequency, and  $V$  is the matrix element coupling the states. A simple calculation yields

$$V = \langle 2P_{1/2} | e\mathbf{E} \cdot \mathbf{r} | 2S_{1/2} \rangle = \sqrt{3}eEa_0/Z, \quad (2)$$

in which  $e$  is the electronic charge,  $a_0$  is the Bohr radius, and  $Z$  is the nuclear charge of the atom.

Equation (1) relates the mean lifetime of the  $2S_{1/2}$

$$\gamma_s = \gamma \left\{ \frac{|V|^2}{\hbar^2(\omega_{bc}^2 + \frac{1}{4}\gamma^2)} + \frac{|M|^2}{\hbar^2(\omega_{ab}^2 + \frac{1}{4}\gamma^2)} + \frac{|V|^4(-3\omega_{bc}^2 + \frac{1}{4}\gamma^2)}{\hbar^4(\omega_{bc}^2 + \frac{1}{4}\gamma^2)^3} + \frac{|V|^2|M|^2(2\omega_{ab}^3\omega_{bc} - 2\omega_{ab}^2\omega_{bc}^2 + 2\omega_{ab}\omega_{bc}^3 + \omega_{ab}\omega_{bc}\gamma^2 + \frac{1}{8}\gamma^4)}{\hbar^4(\omega_{bc}^2 + \frac{1}{4}\gamma^2)^2(\omega_{ab}^2 + \frac{1}{4}\gamma^2)^2} \right\}, \quad (5)$$

where

$$|M| = \langle 2P_{3/2} | e\mathbf{E} \cdot \mathbf{r} | 2S_{1/2} \rangle = (\sqrt{6})eEa_0/Z \quad (6)$$

is the matrix element coupling the state  $2S_{1/2}$  with  $2P_{3/2}$  and  $\omega_{a,b}$ , the level difference between the two states in frequency. This is then the expression used for the determination of  $\omega_{bc}$  from the measured value  $\gamma_s$ .

The effect of hyperfine structure turns out to be a small correction to these results (according to Appendix B). It is thus neglected in the calculation.

The constants required in Eqs. (2), (5), and (6) are

$$(a) \quad \gamma = 1/\tau(2P) = 10^{11}/1.9701$$

as calculated in electric dipole approximation,<sup>18</sup>

$$(b) \quad \hbar = 1.05443 \times 10^{-27} \text{ erg sec,}$$

$$(c) \quad e = 4.80286 \times 10^{-10} \text{ esu,}$$

$$(d) \quad a_0 = 5.29172 \times 10^{-9} \text{ cm,}$$

$$(e) \quad \omega_{ac} = \omega_{ab} + \omega_{bc} = 10\,971.6Z^4 \text{ Mc/sec,}$$

where (e) gives the level difference between  $2P_{3/2}$  and  $2P_{1/2}$ ,  $\omega_{ac}$  from the corresponding value determined by Lamb *et al.*<sup>19</sup> for  $H^2$ , corrected for the differences in charge  $Z$  and reduced mass  $Mm/(M+m)$ .

It must be emphasized that this experimental method is based upon the validity of Eq. (5). Any inaccuracy in the perturbation calculation will be reflected into the determined values of the Lamb shift.

state  $\tau(2S) = 1/\gamma_s$  with the lifetime of the  $2P$  state  $\tau(2P) = 1/\gamma$  and the Lamb shift  $S(=\omega_{bc}/2\pi)$ . Let

$$\delta = 2\sqrt{3}eEa_0/ZS. \quad (3)$$

Then

$$\tau(2S) \approx \tau(2P)(4/\delta^2), \quad (4)$$

when the radiative width  $\gamma^2/4$  is neglected. This is the expression used for the determination of  $S$  from  $\tau(2S)$  in our earlier publication.

Equation (1) neglects two important factors which must be taken into account for more accurate determination of the Lamb shift. These factors are (1) the mixing of the  $2P_{3/2}$  state in addition to that of  $2P_{1/2}$  state, and (2) terms of higher-order approximation. These effects can be taken into account by using the equations of the Bethe-Lamb time-dependent perturbation theory of the Stark mixing of three levels.<sup>17</sup> Referring to the level diagram in Fig. 3 the details of the calculation given in Appendix A, the decay probability, including the effect of Stark mixing of  $2P_{3/2}$ -state and higher-order terms, is

### III. APPARATUS AND EXPERIMENTAL PROCEDURE

#### A. General

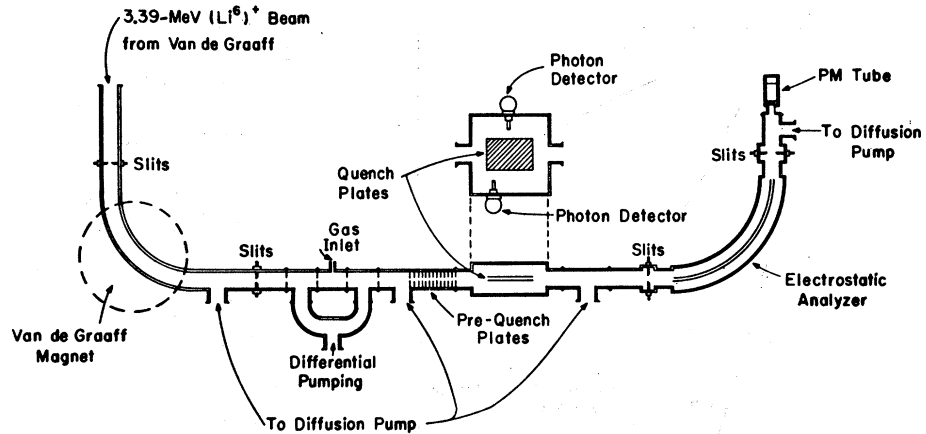
A schematic diagram of the apparatus is shown in Fig. 4. Lithium ions from a lithium source are accelerated to about 3-MeV kinetic energy with the Van de Graaff generator of the University of Chicago. The  $(Li^6)^+$  component is selected with a magnetic analyzer. It passes through a nitrogen-filled charge-exchange cell in which the beam reaches its charge equilibrium. The emerging beam contains about 70% of  $Li^{++}$  ions and 1%  $Li^+$  ions. The rest of the beam consists of  $Li^{++}$  ions and some of them are in the metastable  $2S_{1/2}$  state. The beam then passes through a prequenching region where a longitudinal electrical field of some 15 kV/cm can be applied before the beam enters the observation chamber. In the observation chamber, which is separated from the charge-exchange cell by about 50 cm, a quenching voltage mixes the  $2S_{1/2}$ ,  $2P_{1/2}$ , and  $2P_{3/2}$  states of the originally metastable ions, and 135 Å photons are emitted during the subsequent decay to the ground state. These photons are observed with two photon counters, one stationary for monitoring the photon intensity from the beam shortly after the beam enters the quenching field, while the other is movable for measuring the photon intensity at variable separations from the first.

<sup>17</sup> See Ref. 3, pp. 271-273.

<sup>18</sup> H. Bethe, Phys. Rev. **72**, 339 (1947).

<sup>19</sup> See Ref. 6.

FIG. 4. Schematic diagram of the apparatus used for the experiment.



The application of the prequenching voltage destroys all the metastable ions before they reach the observation chamber. Thus, the counting rates registered by the photon counters with the prequenching voltage "on" condition are due to background. The background counts arise mostly from cosmic rays, x rays from the Van de Graaff accelerator, and radiation produced by the beam in the residual gas of the observation chamber. For each datum point, the counting rates of the two counters are recorded for both prequenching voltage "off" and "on" conditions.

Let  $C_s(\text{off})$  and  $C_s(\text{on})$  denote the counting rates of the stationary counter and  $C_m(\text{off})$  and  $C_m(\text{on})$  denote the moving counter rates during "off" and "on" conditions, respectively.

$$R = \frac{C_m(\text{off}) - C_m(\text{on})}{C_s(\text{off}) - C_s(\text{on})} \quad (7)$$

is then the ratio of the counting rates due to metastable states quenched by the observation chamber electrostatic field at a given separation  $x$  between the two counters. This ratio is normalized to a fixed ion beam current. The plot of  $\ln R$  versus  $x$  should be a straight line if the ions have a single lifetime, and the slope of the straight line is the measure of the decay length of the  $2S_{1/2}$  ions in the applied dc field. The lifetime of the  $2S_{1/2}$  atom is then the decay length divided by the velocity of the ions. A precise measurement of the beam energy and beam composition is done with an electrostatic analyzer after the beam emerges from the observation chamber as shown in Fig. 4.

The normalization of the movable-counter counting rates to the stationary counting rates makes the measurement independent of any change in the beam intensity during the measuring time. However, the background determined with prequenching "on" and quenching "on" has to be referred to the same beam intensity as the signal-plus-background measurement with prequenching "off" and quenching "on." This is accomplished by a careful monitoring of the beam current intensity at the entrance of the electrostatic analyzer. The beam intensity as a function of the time during each run is measured with an electrometer and graphically followed with an automatic recorder.

## B. The Ion Beam

The Li source for the Van de Graaff generator is identical to that described by Allison and Kamegai.<sup>20</sup> The energy resolution of the beam is controlled by the size of the slits of the magnetic analyzer. Higher energy resolution will then naturally result in lower beam intensity. A compromise energy resolution of  $\sim 0.4\%$  was chosen. As discussed in Sec. II, the Lamb shift is approximately proportional to  $[\tau(2S)/\tau(2P)]^{1/2}$ . An uncertainty in the beam energy of  $\pm 0.2\%$  would thus result in an uncertainty of  $\pm 0.05\%$  in the Lamb shift. This was sufficient for our experiment.

The beam-energy profile was measured with the electrostatic analyzer after it emerged from the observation chamber. This profile is determined by the energy resolution of the incident beam plus any broadening suffered by the beam in the charge-exchange cell and it is the profile of the beam passing through the observation chamber. Figure 5 shows a typical profile at 2.650 MeV. The resolution is  $\pm 0.2\%$ .

The charge-exchange cell also collimates the ion beam. The emerging beam has an approximately uniform intensity over a circular area 1 mm in diameter.

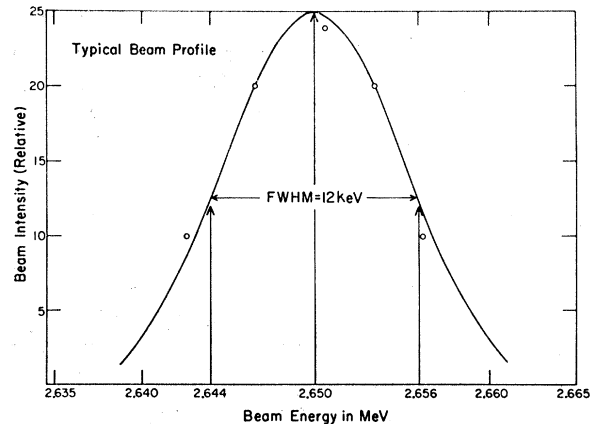


FIG. 5. Profile of the  $\text{Li}^+$  ion beam from the Van de Graaff accelerator.

<sup>20</sup> S. K. Allison and M. Kamegai, Rev. Sci. Instr. **32**, 1090 (1963).

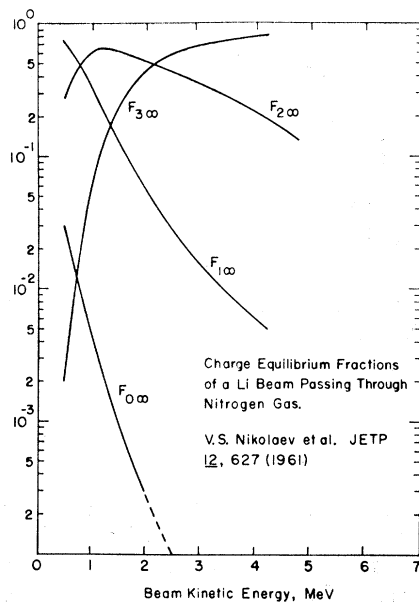


FIG. 6. Charge equilibrium fractions of a Li beam as a function of the energy of the ions.  $F_{0\infty}$ ,  $F_{1\infty}$ ,  $F_{2\infty}$ , and  $F_{3\infty}$  stand for the fraction of Li,  $\text{Li}^+$ ,  $\text{Li}^{++}$ , and  $\text{Li}^{+++}$  ions, respectively.

It passes exactly through the center of the prequenching section and then through the observation chamber midway between the quenching plates.

Nitrogen gas is admitted in the charge-exchange cell until the beam reaches charge equilibrium. The relative intensities of the different charge states have been measured as a function of the beam kinetic energy by Nikolaev *et al.*<sup>21</sup> and are shown in Fig. 6. Some values of the equilibrium fractions were measured by us and found to be in agreement with that of Fig. 6.

### C. Prequenching Section

The prequenching section consists of fourteen parallel plates oriented perpendicular to the beam direction. Each plate has a hole  $\frac{1}{4}$  in. in diameter at the center. They are insulated from one another and have 1-cm separation. The plates are alternately maintained at potentials of about 12 kV and ground. This arrangement quenches all but  $\lesssim 1$  part in  $10^4$  of the metastable ions. Thus, the counting rates recorded by the photon counters in the observation chamber should be entirely due to background.

### D. Observation Chamber and the Photon Detectors

Figures 7(a) and 7(b) show the two cross-sectional views of the observation chamber and the detector systems. The quenching plates are rectangular in shape, 4 in. wide and 5 in. long. The parallelism and separation between the two plates were measured with a feeler gauge and a micrometer. Within an error of  $\pm 5 \times 10^{-4}$  cm, the two plates were found to be parallel and had a

separation of 1.0775 cm. The electrostatic quenching field was produced by a highly stabilized Fluke high-voltage power supply. The high voltage was measured to  $\pm 0.02\%$  using a high-precision voltage divider and differential voltmeter.

The location of the fixed counter (monitor) and the initial position of the movable counter were 4 cm downstream from the forward edge of the plates, at which position the electrostatic field is expected to be uniform to better than 1 part in  $10^4$ .<sup>22</sup>

The beam direction between the plate changes slightly from its initial direction due to the action of the electrostatic field, and this effect tends to increase the movable-counter readings. The angle  $\theta$  between the beam direction at a distance  $l$  cm from the forward edge and its initial direction is approximately given by

$$\tan\theta = 10^{-3}(El/T), \quad (8)$$

in which  $E$  is the field strength in kV/cm and  $T$ , the kinetic energy in MeV of the  $\text{Li}^{++}$  ions. Experimental conditions at which this effect is greatest are  $E=9$  kV/cm,  $T=3$  MeV, and  $l=9$  cm. This gives a correction to the counting rate at this position of only 0.06%.

The photon detectors are two cylindrical side-window GM counters filled with  $Q$  gas; they are similar to those described by Ederer.<sup>23</sup> The counter windows are rectangular in shape with dimensions  $\frac{1}{8}$  in.  $\times$   $\frac{1}{4}$  in. The

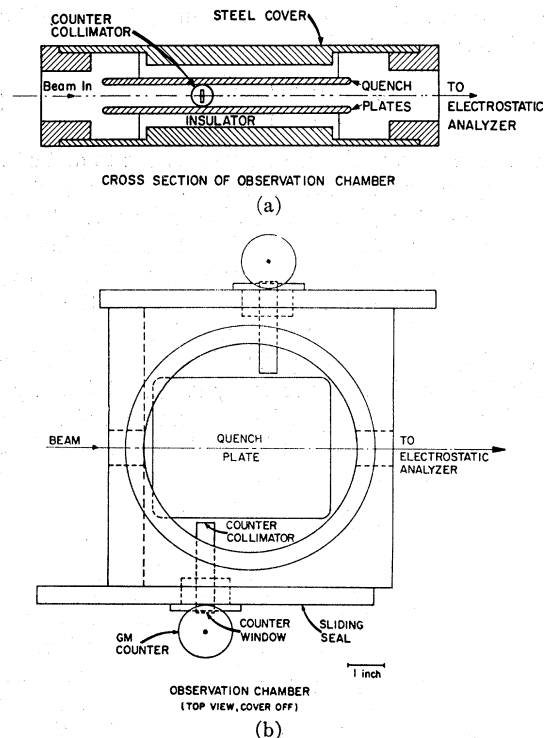


FIG. 7. (a) Cross section of the observation chamber. (b) Top view of the observation chamber.

<sup>21</sup> V. S. Nikolaev, I. S. Dmitriev, L. N. Fateeva, and Ya. A. Teplova, *Zh. Eksperim. i Teor. Fiz.* **39**, 905 (1960) [English transl.: *Soviet Phys.—JETP* **12**, 627 (1961)].

<sup>22</sup> M. E. Rose, *Phys. Rev.* **53**, 715 (1938).

<sup>23</sup> D. L. Ederer, Technical Report No. 9, Department of Physics, Cornell University, Ithaca, New York, 1962 (unpublished).

long dimension is parallel to the counter axis. The view of the counter is limited by a slit, identical in shape and orientation as the counter window situated at a distance of 6.63 cm from the window. In measurement, the slits, which are perpendicular to the beam direction, view a 4-mm-long section of the beam.

The windows of the counters are made of Zapon films of a thickness of about 1000 Å, supported by a 250 mesh nickel screen of 46% transmission. The transmission of the film at 135 Å is  $\sim 74\%$ .<sup>24</sup>

The pressure of the  $Q$  gas in the counters was in general about 80 Torr. Since the gas can gradually diffuse through the Zapon window, a 5-liter reservoir filled with  $Q$  gas at the same pressure as the counters was connected to the counters during the experimental runs. In a 24 h trial there was no measurable change in the gas pressure.

The counters were operated at about 850 V, near the middle of their plateaus. Their characteristics were checked during runs at intervals of 25 min average by introducing a Ra source at a fixed position with respect to the two counters and recording their respective counting rates. In some cases, where the counting efficiency showed a small steady change, this characteristic monitoring allowed to correct the measured counting rates.

### E. The Electrostatic Analyzer

The electrostatic analyzer deflected the beam  $90^\circ$ . After the beam passed the analyzer exit slits it was detected by a scintillator coupled by a light guide to a photomultiplier tube. The scintillator was a CsI(Tl) disk 2.5 cm in diameter and 0.15 cm thick. The detector output was recorded by a counting-rate meter.

The electrostatic analyzer has two concentric plates which are portions of spheres. It is described by Allison *et al.*<sup>25</sup> The two plates were almost symmetrically charged. The beam kinetic energy is given by the

TABLE I. Operational modes, where  $B_0$  are the cosmic rays, radioactive background, and x rays produced by the Van de Graaff accelerator;  $B_1$  are the photons from long-lived excited Li ions other than  $2S$ -state atoms produced in the charge-exchange cell;  $B_2$  are the photons from the residual gas in the observation chamber excited by the ion beam;  $B_3$  are x rays produced by electrons accelerated by the quenching voltage; and  $I$  are photons from quenched metastable atoms.

Mode No.	Beam	Prequenching voltage	Quenching voltage	Origin of detector counts
1	off	off	off	$B_0$
2	on	off	off	$B_0+B_1+B_2$
3	on	off	on	$B_0+B_1+B_2+B_3+I$
4	on	on	on	$B_0+B_1+B_2+B_3$
5	on	on	off	$B_0+B_1+B_2$

<sup>24</sup> D. H. Tombouljian and D. E. Bedo, Rev. Sci. Instr. **26**, 747 (1955).

<sup>25</sup> S. K. Allison, D. Auton, and R. A. Morrison, Phys. Rev. **138**, A688 (1965).

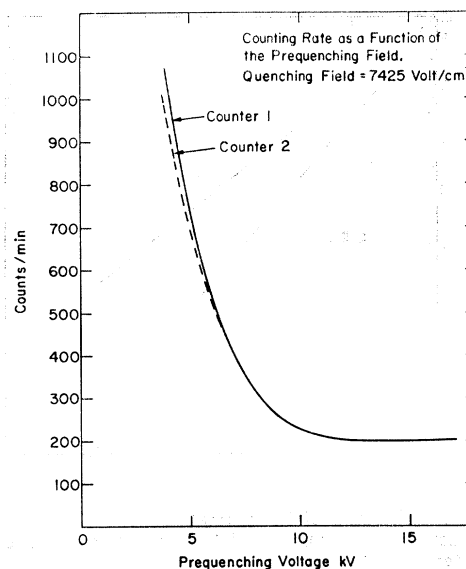


FIG. 8. Counting rates of the fixed counter (No. 1) and that of the movable counter (No. 2) as a function of the prequenching voltage.

equation

$$T = z \left[ K \left( 1 + \frac{Kz(V_2 - V_1)}{2m_0c^2} + \frac{1}{2} \frac{V_2 + V_1}{V_2 - V_1} + 0.00437K \right) \right] \times (V_2 - V_1), \quad (9)$$

where  $z$  is the charge of the ion in units of electronic charge,  $V_2$ ,  $r_2$ , and  $V_1$ ,  $r_1$  are the potentials and radii of the outer and inner plate, respectively,  $m_0$  is the ion rest mass, and

$$K = r_1 r_2 / (r_2^2 - r_1^2) = 80.073. \quad (10)$$

The analyzer slits were 0.025 cm wide and were centered on the tangents to the central orbit between  $r_2$  and  $r_1$ . In this condition, the correction for the entrance and exit fringing field is given by the term 0.00437K.

The plate voltages were measured with a high-precision voltage divider and differential voltmeter. The precision of the analyzer for the measurement of the kinetic energy of the beam is  $\pm 0.15\%$ .

## IV. EXPERIMENTAL RESULTS

### A. Background Subtraction

Table I shows the contributions to the counting rates registered by the detectors in the various operational modes.

Tests were conducted to show that the chosen longitudinal electrostatic prequenching field suppresses practically all the  $\text{Li}^{++}$  ( $2S$ ) metastable ions from the beam. Figure 8 shows the counting rates of both of the fixed and movable counter as a function of the prequenching voltage. The rates decrease to a plateau, representing the background  $B_0+B_1+B_2+B_3$  when the

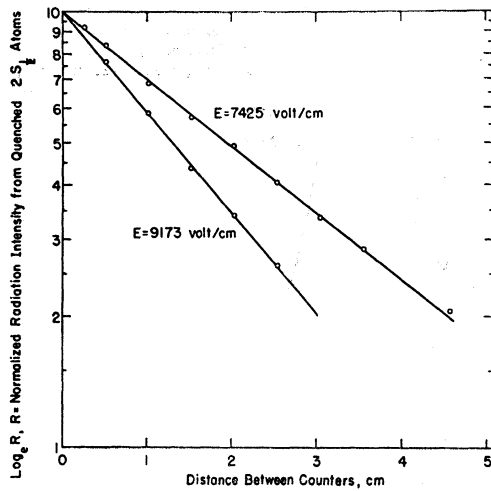


FIG. 9. Semilog plot of the normalized counting rates of the movable counter as a function of the separation  $x$  between the two counters.

prequenching field suppresses all the metastable ions. The working prequenching voltage was chosen to be several kV higher than the onset of the plateau.

Two important requirements for a proper subtraction of the background are that the counting rates of the movable counter in operation mode Nos. 1, 2, 4, and 5 must be independent of the counter position along the quenching plates, and that the counting rates recorded in operation mode No. 2 must be equal to that in mode No. 5. This would be the case if there is only a negligible amount of long-lived excited Li ions other than the  $2S$  atoms and the voltage on the prequenching plates does not produce any excitation in the beam. Tests showed that within statistical fluctuation these conditions were fulfilled.

In the operation mode No. 3,  $I$  is the photon intensity arising from the Stark quenching of the  $\text{Li}^{++}$  ( $2S$ ) atoms. However, it is necessary to show that contributions to  $I$  from metastable atoms of other species such as  $2^1S$   $\text{Li}^+$  ions are negligible.

The experimental curves in Fig. 6 show that the charge-equilibrated beam at the kinetic energies used for the experiments contains about 1.5% of  $\text{Li}^+$ . This small fraction of heliumlike ions may contain metastable atoms in the  $2^1S$  and  $2^3S$  states. The lifetimes of these states of He due to two-photon emission are  $\frac{1}{7}$  sec and  $\gg \frac{1}{7}$  sec,<sup>26</sup> respectively. The triplet is insensitive to the Stark quenching. The singlet state is coupled mainly to the  $2^1P$  state by the field and subsequently decays to the ground state. No information is available either on the cross section for the production of the  $\text{Li}^+$  ( $2^1S$ ) atoms or on the rate of destruction by Stark quenching. However, it is safe to assume that the decay probability under the action of an electric field is smaller than that of the corresponding state in the helium atom because of the larger separation in the atomic levels. The helium  $2^1S$  decay probability has

<sup>26</sup> G. Breit and E. Teller, *Astrophys. J.* **91**, 215 (1940).

been calculated and measured by Holt and Krotov<sup>27</sup>; it is given by

$$\Gamma = (0.89 \pm 0.04) E^2 \text{ sec}^{-1}, \quad (11)$$

where  $E$  is the field strength in kV/cm. Taking this expression as the upper limit for the case of lithium ions, it is found that the decay probability is about  $75 \text{ sec}^{-1}$  at the highest electric field used for the experiments. Making the extreme assumption that all the  $\text{Li}^+$  ions in the beam were in the state  $2^1S$ , the calculated intensity due to the quenching of the metastables contributes only 0.01% to the counting rates. It can thus be neglected.

## B. Experimental Results

Figure 9 shows the plot of  $\ln R$ , where  $R$  is the quantity defined in Eq. (7), as a function of the counter separation  $x$  for two different values of the quenching field, throughout which the experimental conditions were maintained at their best. The first was at a quenching field  $7425 \pm 2 \text{ V/cm}$  whereas the second one was at  $9173 \pm 2 \text{ V/cm}$ . The average standard deviation of the points in Fig. 9 is about 1.5%. The decay lengths determined from the slopes of the straight lines divided by the velocity of the lithium ions yield the mean lifetime of the  $2S$  state for the corresponding field values. Table II shows the results with the correction about 0.06% for the relativistic time dilation included. The averaged Lamb shift  $S$  as calculated from Eq. (5) with these determined lifetimes is

$$S = 63\,031 \pm 327 \text{ Mc/sec.}$$

## V. COMPARISON WITH THEORY

Erickson calculated the Lamb shift in  $(\text{Li}^6)^{++}$ , including higher-order terms in  $(\alpha Z)$ .<sup>28</sup> The results are summarized in Table III, in which  $L$  is the Lamb constant,

$$L = \frac{4\alpha(\alpha)^4 mc^2}{3\pi(2)^{3/2} \hbar} = 135.63355 \pm 0.0058 \text{ Mc/sec,}$$

$\alpha$  is the fine-structure constant,

$$\alpha^{-1} = 137.0388 \pm 0.0019,$$

$M/m$  is the ratio of the mass of  $\text{Li}^6$  to the electronic mass,

$$M/m = 5.970 \times 1836,$$

TABLE II. Lifetime of  $(\text{Li}^6)^{++} 2S_{1/2}$  atoms.

Beam energy (MeV)	Quenching field (V/cm)	Mean lifetime (sec)
$3.343 \pm 0.005$	$7425 \pm 2$	$(2.616 \pm 0.042) \times 10^{-9}$
$3.409 \pm 0.005$	$7425 \pm 2$	$(2.642 \pm 0.042) \times 10^{-9}$
$3.346 \pm 0.005$	$9173 \pm 2$	$(1.764 \pm 0.046) \times 10^{-9}$

<sup>27</sup> H. K. Holt and R. Krotov, *Phys. Rev.* **144**, 82, 1966.

<sup>28</sup> G. W. Erickson, *Phys. Rev. Letters* **15**, 338 (1965).

TABLE III. The  $2^2S_{1/2}-2^2P_{1/2}$  shift for a hydrogenlike atom of nuclear charge  $Z$ .

Contribution	Order	Effect	$2S_{1/2}-2P_{1/2}$ shift for $(\text{Li}^6)^{++}$ (Mc/sec)
Second-order radiative corrections			
$Z^4 L \left( 2 \ln(z\alpha)^{-1} + (m/M) + \frac{1}{2} \frac{1}{4} + \ln \frac{K_0(2.1)}{K_0(2.0)} \right)$			
$\times [1 - 3(m/M)]$	$\alpha(\alpha Z)^4$	Radiative shift	} 61067.6
$Z^4 L \frac{1}{2} [1 - 2.75(m/M)]$	$\alpha(\alpha Z)^4$	Magnetic moment	
$Z^4 L \left(-\frac{1}{5}\right) [1 - 3(m/M)]$	$\alpha(\alpha Z)^4$	Vacuum polarization	
$Z^5 L (3\pi\alpha) \left[1 + \frac{1}{1} \frac{1}{8} - \frac{1}{2} \ln 2 + \frac{5}{1} \frac{5}{8}\right] [1 - 3(m/M)]$	$\alpha(\alpha Z)^5$	Second order in the external potential	1735.0
		Higher order in the external potential	-173.5
Fourth-order radiative corrections			
$Z^4 L \left[\frac{3}{2}(\alpha/\pi)\right] (0.52)$	$\alpha^2(\alpha Z)^4$	Radiative shift	} -19.6
$Z^4 L [-0.328(\alpha/\pi)]$	$\alpha^2(\alpha Z)^4$	Magnetic moment	
$Z^4 L \left[-\frac{4}{5} \frac{1}{4}(\alpha/\pi)\right]$	$\alpha^2(\alpha Z)^4$	Vacuum polarization	
		Finite mass	13.0
		Finite size	117.3
		Total theory	62 739.9 ± 47.1
		Present experiment	63 031 ± 327

and  $\ln[K_0(2, 1)/K_0(2, 0)]$  is the difference between the Bethe logarithms for  $2S$  and  $2P$  states,

$$\ln[K_0(2, 1)/K_0(2, 0)] = -2.841786580.$$

The theoretical value is

$$S(\text{theory}) = 62739.0 \pm 47.1 \text{ Mc/sec},$$

which appears to be in agreement with the experimental result within the uncertainty quoted in this paper.<sup>29</sup>

#### ACKNOWLEDGMENTS

We wish to express our sincere appreciation to Professor J. A. Simpson for his interest in this work and for providing laboratory facilities for all phases of the experiments. This work was initiated by the encouragement of the late Professor S. K. Allison.

#### APPENDIX A: CONNECTION BETWEEN THE DECAY PROBABILITY OF THE $2S_{1/2}$ STATE AND THE LAMB SHIFT

Referring to the energy-level diagram in Fig. 3, the probability amplitude for each of the three levels of a hydrogenlike atom of nuclear charge  $Z$  are denoted by letters  $a$ ,  $b$ , and  $c$ , respectively. The equations of

<sup>29</sup> In our earlier publication (Ref. 14), the experimental Lamb shift was stated as 62 300 Mc/sec. It was computed from an expression which does not include the contribution from the mixing of  $2P_{3/2}$  state and that from higher-order terms. By using the refined expression in this paper, the measured lifetime yields the value for the Lamb shift as 62 700 Mc/sec. It is in agreement with the values reported in this paper.

time-dependent perturbation theory, following Lamb's treatment, are

$$\begin{aligned} i\hbar\dot{a} &= -\frac{1}{2}i\hbar\gamma a + Mb \exp(i\omega_{ab}t), \\ i\hbar\dot{b} &= M^*a \exp(-i\omega_{ab}t) + V^*c \exp(i\omega_{bc}t), \\ i\hbar\dot{c} &= Vb \exp(-i\omega_{bc}t) - \frac{1}{2}i\hbar\gamma c. \end{aligned} \quad (12)$$

In Eq. (12), the quantities  $\omega_{ab}$  and  $\omega_{bc}$  are the circular frequency separations of states  $a$  and  $b$ , and  $b$  and  $c$ , respectively,  $\gamma$  is the radiative width of the  $P$  states, and  $V$  and  $M$  are the matrix elements coupling the level  $b$  to  $c$  and  $a$ , respectively. A simple calculation shows that

$$V = (2P_{1/2} | e\mathbf{E} \cdot \mathbf{r} | 2S_{1/2}) = \sqrt{3}eEa_0/Z$$

and

$$M = (2P_{3/2} | e\mathbf{E} \cdot \mathbf{r} | 2S_{1/2}) = (\sqrt{6})eEa_0/Z, \quad (13)$$

in which  $e$  is the electronic charge,  $a_0$  is the Bohr radius, and  $Z$  is the nuclear charge of the atom. The levels  $a$  and  $c$  are not coupled because they have the same parity.

Equations (12) have a general solution

$$\begin{aligned} a &= \sum_{k=1}^3 A_k \exp(i\omega_{ab} - \mu_k)t, \\ b &= \sum_{k=1}^3 B_k \exp(-\mu_k t), \\ c &= \sum_{k=1}^3 C_k \exp(-i\omega_{ac} - \mu_k)t, \end{aligned} \quad (14)$$

where the  $\mu_k$ 's satisfy the following equation:

$$\hbar^2 \mu_k (i\omega_{ab} - \mu_k + \frac{1}{2}\gamma) (-i\omega_{bc} - \mu_k + \frac{1}{2}\gamma) = M^2 (-i\omega_{bc} - \mu_k + \frac{1}{2}\gamma) + |V|^2 (i\omega_{ab} - \mu_k + \frac{1}{2}\gamma). \quad (15)$$

The quantities  $\mu_k + \mu_k^*$  essentially determine the rate of decay of each of the three levels in the mixture. To the zeroth-order approximation,

$$\mu_1 = i\omega_{ab} + \frac{1}{2}\gamma, \quad \mu_2 = 0, \quad \mu_3 = -i\omega_{bc} + \frac{1}{2}\gamma. \quad (16)$$

Two of these,  $\mu_1 + \mu_1^*$  and  $\mu_3 + \mu_3^*$ , correspond to the radiative decay probability  $\gamma$  of the unperturbed  $2P$

$$\begin{aligned} \gamma_s = \mu_2 + \mu_2^* \\ = \gamma \left\{ \frac{|V|^2}{\hbar^2(\omega_{bc}^2 + \frac{1}{4}\gamma^2)} + \frac{|M|^2}{\hbar^2(\omega_{ab}^2 + \frac{1}{4}\gamma^2)} + \frac{|V|^4(-3\omega_{bc}^2 + \frac{1}{4}\gamma^2)}{\hbar^4(\omega_{bc}^2 + \frac{1}{4}\gamma^2)^3} \right. \\ \left. + \frac{|V|^2|M|^2(2\omega_{ab}^3\omega_{bc} - 2\omega_{ab}^2\omega_{bc}^2 + 2\omega_{bc}^3\omega_{ab} + \omega_{ab}\omega_{bc}\gamma^2 + \frac{1}{8}\gamma^4)}{\hbar^4(\omega_{bc}^2 + \frac{1}{4}\gamma^2)^2(\omega_{ab}^2 + \frac{1}{4}\gamma^2)^2} \right\}. \quad (18) \end{aligned}$$

This equation gives the connection between the Lamb shift  $\omega_{bc}$  and the decay probability  $\gamma_s$ .

It should be noted that the energy levels of the atom are all shifted due to the Stark effect. The changes in the  $2P_{3/2}$ ,  $2S_{1/2}$ , and  $2P_{1/2}$  levels can be conveniently obtained as follows: The quantities  $(1/2i)(\mu_k - \mu_k^*)$  determine the level differences relative to  $2S_{1/2}$  including the shift in levels due to Stark effect. In the zeroth-order approximation, the level differences of  $a$ ,  $b$ , and  $c$  according to Eq. (16) were  $\omega_{ab}$ , 0, and  $-\omega_{bc}$ . To the first order of approximation,

$$\mu_1 = i\omega_{ab} + \frac{1}{2}\gamma \frac{|M|^2}{\hbar^2(i\omega_{ab} + \frac{1}{2}\gamma)}, \quad (19)$$

and

$$\mu_3 = -i\omega_{bc} + \frac{1}{2}\gamma - \frac{|V|^2}{\hbar^2(-i\omega_{bc} + \frac{1}{2}\gamma)}. \quad (20)$$

The level differences are then

$$(2i)^{-1}(\mu_1 - \mu_1^*) = \omega_{ab} \left\{ 1 + \frac{|M|^2}{\hbar^2(\omega_{ab}^2 + \frac{1}{4}\gamma^2)} \right\}, \quad (21)$$

$$(2i)^{-1}(\mu_2 - \mu_2^*) = \frac{|V|^2\omega_{bc}}{\hbar^2(\omega_{bc}^2 + \frac{1}{4}\gamma^2)} - \frac{|M|^2\omega_{ab}}{\hbar^2(\omega_{ab}^2 + \frac{1}{4}\gamma^2)}, \quad (22)$$

$$(2i)^{-1}(\mu_3 - \mu_3^*) = -\omega_{bc} \left\{ 1 + \frac{|V|^2}{\hbar^2(\omega_{bc}^2 + \frac{1}{4}\gamma^2)} \right\}. \quad (23)$$

Thus the shift due to the Stark effect for the  $2P_{3/2}$ ,  $2S_{1/2}$ , and  $2P_{1/2}$  levels are, respectively,

$$\begin{aligned} \Delta_a &= \frac{|M|^2\omega_{ab}}{\hbar^2(\omega_{bc}^2 + \frac{1}{4}\gamma^2)}, \\ \Delta_b &= \frac{|V|^2\omega_{bc}}{\hbar^2(\omega_{bc}^2 + \frac{1}{4}\gamma^2)} - \frac{|M|^2\omega_{ab}}{\hbar^2(\omega_{ab}^2 + \frac{1}{4}\gamma^2)} = -\Delta_a - \Delta_c, \\ \Delta_c &= -\frac{|V|^2\omega_{bc}}{\hbar^2(\omega_{bc}^2 + \frac{1}{4}\gamma^2)}. \quad (24) \end{aligned}$$

states, whereas  $\mu_2 + \mu_2^* = 0$  is the decay probability of the  $2S_{1/2}$  state induced by the Stark mixing in the zero-order approximation.

To an approximation sufficient for the present purpose,

$$\begin{aligned} \mu_2 &= \frac{|V|^2}{\hbar^2(-i\omega_{bc} + \frac{1}{2}\gamma)} + \frac{|M|^2}{\hbar^2(i\omega_{ab} + \frac{1}{2}\gamma)} \\ &+ \frac{(i\omega_{ab} - i\omega_{bc} + \gamma)|V|^2|M|^2}{\hbar^4(-i\omega_{bc} + \frac{1}{2}\gamma)^2(i\omega_{ab} + \frac{1}{2}\gamma)^2} + \frac{|V|^4}{\hbar^4(-i\omega_{bc} + \frac{1}{2}\gamma)^3}. \quad (17) \end{aligned}$$

Consequently,

## APPENDIX B: CORRECTIONS FOR HYPERFINE STRUCTURE

The one remaining effect to be considered is that of hyperfine structure. It is assumed that the quantity of  $\mu_2 + \mu_2^*$  can be broken up into contributions from each of the possible hyperfine transitions. Only the change in the energy  $\omega_{bc}$  as a result of hyperfine splittings will be taken into account. Since the nuclear spin in  $\text{Li}^6$  is 1, each fine-structure level splits into two hyperfine components  $F = \frac{3}{2}$  and  $F = \frac{1}{2}$ . The  $F = \frac{3}{2}$  levels are raised in energy relative to the fine-structure level by about 353 and 118 Mc/sec, whereas the  $F = \frac{1}{2}$  levels are lowered by 706 and 236 Mc/sec for the  $2S_{1/2}$  and  $2P_{1/2}$  levels, respectively. There are thus four possible combinations of a  $2S_{1/2}$  hyperfine level with a  $2P_{1/2}$  hyperfine level. In order to break up  $\mu_2 + \mu_2^*$  into properly weighted contributions from each of the combinations, it is necessary to know the square of the matrix element

$$\begin{aligned} \sum_{m_F'} | (2P_{1/2}F'm_F' | e\mathbf{E} \cdot \mathbf{r} | 2S_{1/2}Fm_F) |^2 \\ = | (2P_{1/2}F'm_F' | e\mathbf{E} \cdot \mathbf{r} | 2S_{1/2}Fm_F) |^2. \quad (25) \end{aligned}$$

The sum reduced to one term because  $m_F$  is a good quantum number. It is possible to show<sup>30</sup> that the square of this matrix element is proportional to  $m^2$  if  $F = F'$ , and to  $(\frac{3}{2})^2 - m^2$  if  $F \neq F'$ . Thus the relative intensity of  $F' = F = \frac{3}{2}$ ,  $m_F = \frac{3}{2}$ , is  $\frac{9}{4}$ ; that of  $F' = F = \frac{3}{2}$ ,  $m_F = \frac{1}{2}$ , is  $\frac{1}{4}$ ; and that of  $F' = \frac{1}{2}$ ,  $F = \frac{3}{2}$ ,  $m_F = \frac{1}{2}$ , is  $\frac{3}{4}$ . It is noted that the sum of the squares of the matrix elements over both values of  $F'$  gives  $\frac{9}{4}$  and is independent of both  $F$  and  $m_F$ . After normalizing the weight assigned to each of the possible hyperfine transitions, one arrives at the following partition of  $\mu_2 + \mu_2^*$ :

$$\mu_2 + \mu_2^* = \gamma_2 = \frac{1}{2}\gamma_1 + \frac{8}{2}\gamma_2 + \frac{8}{2}\gamma_3 + \frac{1}{2}\gamma_4. \quad (26)$$

<sup>30</sup> These matrix elements were evaluated explicitly with the kind assistance of Dr. Daniel Zwanziger at New York University.

The quantity  $\gamma_1$  is the Stark-induced decay rate involving the hyperfine levels separated by  $\omega_{bc}+353-118=\omega_{bc}+235$  Mc/sec;  $\gamma_2$ , the rate involving  $\omega_{bc}+353+235=\omega_{bc}+588$  Mc/sec;  $\gamma_3$ , the rate involving  $\omega_{bc}-706-118=\omega_{bc}-824$  Mc/sec, and  $\gamma_4$ , the rate involving  $\omega_{bc}-706+235=\omega_{bc}-471$  Mc/sec.

Equation (18) may then be used to relate each one of the  $\gamma_i$  to the appropriate energy separation;  $\mu_2+\mu_2^*$  is then obtainable from Eq. (26). At 7425 V/cm, the result of this procedure is that  $\tau(2S)$  is decreased by only about 3 parts in  $10^4$  which is then neglected for the present purpose.

## Hyperfine Structure of the $v=0, J=1$ State in $Rb^{85}F, Rb^{87}F, K^{39}F,$ and $K^{41}F$ by the Molecular-Beam Electric-Resonance Method\*†

P. A. BONCZYK‡ AND V. W. HUGHES

Gibbs Laboratory, Yale University, New Haven, Connecticut

(Received 31 October 1966; revised manuscript received 27 June 1967)

The electric and magnetic interactions which determine the hfs of the  $v=0, J=1$  state in  $Rb^{85}F, Rb^{87}F, K^{39}F,$  and  $K^{41}F$  have been obtained from spectra measured in zero magnetic field and near zero electric field. A molecular-beam electric-resonance apparatus with two-wire-type focusing fields and a single 30-cm transition field was used. For  $Rb^{85}F$  and  $Rb^{87}F$  the electric quadrupole interaction constants are  $(eq_1Q_1)/h = (-70.3405 \pm 0.0004)$  Mc/sec and  $(eq_1Q_1)/h = -(34.0313 \pm 0.0010)$  Mc/sec, respectively. Hence the ratio of the Rb nuclear quadrupole moments is  $Q_{85}/Q_{87} = +(2.06694 \pm 0.00006)$ . Comparison with data on the electric quadrupole interaction constants for  $Rb^{85}Cl$  and  $Rb^{87}Cl$  gives no evidence of a contribution from nuclear electric polarization. In  $Rb^{85}F$ , the constant of the spin-rotation interaction involving the Rb nucleus  $c_1(I_1 \cdot J)$  is  $c_1/h = +(0.525 \pm 0.010)$  kc/sec, the constant of the spin-rotation interaction involving the F nucleus  $c_2(I_2 \cdot J)$  is  $c_2/h = +(10.53 \pm 0.07)$  kc/sec, and the constant of the electron-coupled nuclear dipole-dipole scalar interaction  $c_4(I_1 \cdot I_2)$  is  $c_4/h = +(0.23 \pm 0.06)$  kc/sec. In  $Rb^{87}F$ , these interaction constants are  $c_1/h = +(1.595 \pm 0.050)$  kc/sec,  $c_2/h = +(10.51 \pm 0.08)$  kc/sec, and  $c_4/h = +(0.66 \pm 0.10)$  kc/sec. The Hamiltonian also includes a nuclear dipole-dipole tensor term, and the interaction constants are  $c_3/h = +(0.93 \pm 0.05)$  kc/sec and  $c_3/h = +(3.16 \pm 0.18)$  kc/sec in  $Rb^{85}F$  and  $Rb^{87}F$ , respectively. These agree very well with values calculated from  $(g_1 g_2 \mu_N^2 \langle R^{-3} \rangle_{n,v}/h)$ , so that there is no evidence for a tensor part of the electron-coupled nuclear dipole-dipole interaction in RbF. The electric quadrupole interaction constants are  $(eq_1Q_1)/h = -(7932.9 \pm 0.2)$  kc/sec and  $(eq_1Q_1)/h = -(9656.9 \pm 0.6)$  kc/sec for  $K^{39}F$  and  $K^{41}F$ , respectively. The ratio of the K nuclear quadrupole moments is  $Q_{39}/Q_{41} = +(0.8215 \pm 0.0001)$ . The observed  $K^{39}F$  spectrum also allowed the determination of the interaction constants:  $c_1/h = (270 \pm 20)$  cps;  $c_2/h = (10.67 \pm 0.08)$  kc/sec;  $c_3/h = (540 \pm 70)$  cps;  $c_4/h = (30 \pm 80)$  cps. We point out that experimental evidence for nuclear polarizability of Br nuclei is provided by data of others on the electric quadrupole interaction constants of  $Br^{79}$  and  $Br^{81}$  in the Br atom and in LiBr.

### INTRODUCTION

THIS paper is divided into two parts. The first part reports a high-precision measurement of the molecular hyperfine structure of the  $Rb^{85}F$  and  $Rb^{87}F$  molecules in the vibrational state  $v=0$  and the rotational state  $J=1$ , done by the molecular-beam electric-resonance method. This experiment is a much improved version of an older experiment by Hughes and Grabner.<sup>1</sup> The resolution achieved in the present experiment represents a factor of 10 improvement over the older experiment, and hence individual lines which were previously unresolved are now resolved. The second

part reports briefly on results for  $K^{39}F$  and  $K^{41}F$ . Preliminary reports of the results of the present experiment were given earlier.<sup>2</sup>

The radio-frequency spectrum observed is completely accounted for by a Hamiltonian which includes the electric quadrupole interaction with the Rb nucleus, the spin-rotation interactions with coupling constants  $c_1$  and  $c_2$  for Rb and F respectively, the nuclear dipole-dipole tensor interaction with coupling constant  $c_3$ , and the scalar part of the electron-coupled nuclear dipole-dipole interaction with coupling constant  $c_4$ . The constants  $c_1, c_3,$  and  $c_4$  are determined for the first time in the RbF molecules.<sup>2</sup> The new values for the electric quadrupole interaction constants and for  $c_2$  are more precise than the older values<sup>1</sup> by a factor of about 100 and the sign of  $c_2$  is now determined.

\* This research was supported in part by the National Aeronautics and Space Administration and by the U.S. Air Force Office of Scientific Research.

† Submitted by P. A. Bonczyk in partial fulfillment of the requirements for the Ph.D. degree in Physics at Yale University.

‡ Present address: Physics Department, Massachusetts Institute of Technology, Cambridge, Massachusetts.

<sup>1</sup> V. W. Hughes and L. Grabner, Phys. Rev. **79**, 314 (1950).

<sup>2</sup> P. A. Bonczyk and V. W. Hughes, Bull. Am. Phys. Soc. **9**, 452 (1964); **10**, 101 (1965); P. A. Bonczyk, *ibid.* **132** (1967).